Quantitative Label-Free Imaging of Lipid Composition and Packing of Individual Cellular Lipid Droplets Using Multiplex CARS Microscopy

Hilde A. Rinia,* Koert N. J. Burger,[†] Mischa Bonn,[‡] and Michiel Müller*

*Swammerdam Institute for Life Sciences, University of Amsterdam, 1098 SM Amsterdam, The Netherlands; [†]Division of Endocrinology and Metabolism, Department of Biology and Institute of Biomembranes, Utrecht University, 3584 CH Utrecht, The Netherlands; and [‡]FOM Institute for Atomic and Molecular Physics (AMOLF), Kruislaan 407, 1098 SJ Amsterdam, The Netherlands

ABSTRACT Lipid droplets (LDs) are highly dynamic organelles that perform multiple functions, including the regulated storage and release of cholesterol and fatty acids. Information on the molecular composition of individual LDs within their cellular context is crucial in understanding the diverse biological functions of LDs, as well as their involvement in the development of metabolic disorders such as obesity, type II diabetes, and atherosclerosis. Although ensembles of LDs isolated from cells and tissues were analyzed in great detail, quantitative information on the heterogeneity in lipid composition of individual droplets, and possible variations within single lipid droplets, is lacking. Therefore, we used a label-free quantitative method to image lipids within LDs in 3T3-L1 cells. The method combines submicron spatial resolution in three dimensions, using label-free coherent anti-Stokes Raman scattering microscopy, with quantitative analysis based on the maximum entropy method. Our method allows quantitative imaging of the chemistry (level of acyl unsaturation) and physical state (acyl chain order) of individual LDs. Our results reveal variations in lipid composition and physical state between LDs contained in the same cell, and even within a single LD.

INTRODUCTION

Organisms ranging from bacteria to plants and animals have developed an efficient means of storing energy for times of food deprivation: fatty acids are stored as neutral lipids, mainly triacylglycerol, densely packed in lipid droplets (LDs) inside cells (1). In recent years, it has become clear that LDs are highly dynamic organelles (2,3) with multiple and very diverse functions, not only in storing energy, but also in the regulation of cholesterol homeostasis, in the biosynthesis of membrane lipids, steroid hormones, and eicosanoids, and as a transient storage compartment of proteins (4–6). Although in mammals, LDs are mainly found in adipocytes, LD formation is not restricted to any particular cell type. Indeed, LDs appear to be a universal component of cellular lipid homeostasis, and all cell types studied so far have the ability to form LDs when confronted with elevated levels of fatty acids. In obesity, the maximum capacity of adipose tissue to store fatty acids as triacylglycerol may be exceeded, resulting in elevated fatty-acid levels in the blood and accumulation of triacylglycerol in nonadipose tissues such as liver and skeletal muscle (so-called ectopic fat). The gradual accumulation of ectopic fat in obese subjects interferes with local insulin signaling, and plays a key role in the development of type 2 diabetes, which is becoming a major public health threat (7).

Understanding the diverse biological functions of LDs and their role in the development of metabolic diseases requires detailed information on both the protein and lipid composition of individual LDs within their cellular context. An important parameter is the number of double C = C bonds within lipid acyl chains, i.e., the degree of unsaturation. Clearly, quantitative spatial and temporal information on the degree of lipid unsaturation would greatly contribute to our understanding of metabolic diseases and the influence of nutritional factors. For instance, there is accumulating evidence that insulin sensitivity is affected by the quality of dietary fat, acyl chain length, and degree of unsaturation, independent of the effect of lipid intake on body weight (8), but the underlying mechanisms at the cellular level have not been resolved.

Studies on the chemistry of endogenous lipids in LDs have remained largely limited to the characterization of bulk samples, composed of ensembles of LDs, isolated from cells or tissues (9,10). The importance of analyzing single particles instead of bulk samples was clearly demonstrated in a Raman spectroscopy study on single triacylglycerol-rich lipoprotein particles isolated from human blood, which revealed considerable heterogeneity in lipid composition between individual lipoprotein particles (11). Importantly, microscopic techniques based on vibrational spectroscopy, such as Raman spectroscopy, provide images without the need for labeling; the contrast is generated by differences in chemical and physical properties between endogenous molecules. In LDs, the most evident and important difference in chemistry is the presence or absence of double bonds, i.e., the level of unsaturation of acyl chains. In recent years, (confocal) Raman

microscopy has evolved as a very useful tool in this area of research, and various biological samples, including LD-containing cells, have been imaged (12–22). Particularly noteworthy in the context of this study are recent reports of applications of coherent anti-Stokes Raman scattering (CARS) microscopy to LD research (17–23). These results demonstrated that CARS microscopy can provide detailed insights into the cellular biochemistry of fat molecules. However, it has not been possible to investigate quantitatively variations in local lipid composition between or within LDs. We show here that multiplex CARS, in conjunction with appropriate spectral-analysis tools, allows a determination of the local composition and organization of lipids in LDs in a noninvasive, label-free manner. The essence of the approach is that for each submicron pixel, a CARS spectrum is recorded within 20 ms. Spectra are analyzed using an approach (24) that allows a quantification of densities, chemical composition, and physical state within LDs.

Compared with spontaneous Raman scattering, the main advantages of using multiplex CARS include higher signal strengths (the CARS signal is stronger by ~4 orders of magnitude) and related shorter acquisition times, and the absence of autoluminescence within the detection window. Moreover, the CARS signal is coherently emitted in a direction determined by phase-matching, allowing for efficient detection. The third-order dependence of the CARS signal on the input laser intensity provides inherent optical sectioning capability. Using multiplex CARS, the signal enhancement relative to Raman scattering permits acquisition times over the full spectral window as short as 20 ms. In fact, for the experiments presented here, the acquisition time for spectral imaging in the CH-stretch spectral window was limited by the CCD camera, rather than by the signal itself. These short acquisition times allow for rapid generation of spectral images of various parts of a cell, within a single cell culture or from a number of cell cultures, yielding statistically significant data. Because the CARS signal is coherent and generated on the high-frequency side of the laser, the recorded signal is free from disturbances because of autoluminescence of the sample. This latter factor often complicates (and may prohibit) the use of Raman spectroscopy in biological imaging. We carefully examined possible photodamage to cells in these multiplex CARS experiments, but found no indications of induced damage.

To demonstrate the potential of multiplex CARS microscopy in the analysis of LDs, we incubated differentiated mouse adipocytes (3T3-L1 cells) with a series of well-defined mixtures of saturated and unsaturated fatty acids. By combining CARS microscopy with quantitative spectral analysis, using a phase-retrieval algorithm based on the maximum entropy method (MEM), we generated high-resolution spectral images displaying the chemical composition (level of acyl-chain unsaturation) and physical state (acyl-chain order) of individual LDs in their cellular context. Our results reveal a remarkable degree of heterogeneity in these parameters between, and even within, LDs in adipocytes. The results depended critically on the fatty-acid composition of the incubation mixture. Moreover, we present evidence suggesting that newly synthesized triacylglycerol is first deposited in small LDs and not directly in the large preexisting LDs in adipocytes.

The data presented here were collected at room temperature on mildly fixed cells. In addition, we verified that the same behavior (e.g., phase separation within LDs) was observed at physiological temperatures (37°C) for living cells. Fixing cells facilitates measurements, allowing for better statistics. In the fixation procedure, the use of organic solvents and hydrophobic mounting media were avoided (see the Supplementary Material, Data S1). This method was previously shown to preserve cellular lipid content and not affect LD morphology, at least at the light-microscopy level (25). An example of multiplex CARS microscopy on living cells is shown in Movie S1, demonstrating the possibility of following processes such as LD formation and breakdown in real time.

METHODS

Multiplex CARS microscopy

Imaging experiments were performed with a multiplex CARS microscopy setup, consisting of two tunable mode-locked Ti/sapphire lasers (Tsunami, Spectra Physics) with a repetition rate of 82 MHz, which were made collinear and synchronized ("lok-to-clock", Spectra Physics, Mountain View, CA). An additional home-built, long-term feedback system ensured a timing jitter between the lasers of <1 ps. The pump/probe laser provides 10-ps pulses (bandwidth, 1.5 cm^{-1} full width at half-maximum) centered at 710 nm. The *Stokes* laser produces 80-fs pulses (bandwidth, ~180 cm^{-1} full width at half-maximum) with a center wavelength tunable between 750–950 nm, corresponding to the vibrational range of ~750–3500 cm^{-1}. Typical average powers used in the sample were ~20 mW and ~3 mW for the pump/probe and Stokes laser, respectively. Achromatic $\lambda/2$ plates and polarizers ensured all-parallel polarization conditions for pump, Stokes, probe, and anti-Stokes. Laser beams were focused with a microscope objective (63×/1.2 numerical aperture (NA) oil immersion; Zeiss, Jena, Germany) into the sample, which was contained between two cover glasses. The multiplex CARS signal was collected in the forward direction, using another microscope objective (40×/0.6 NA; Zeiss), filtered by a short wave pass and a 710-nm Notch filter, and spectrally resolved on a spectrometer (*MS257*; Oriel, Mountain View, CA), equipped with a CCD camera (Andor, Belfast, Northern Ireland) with an effective spectral resolution of ~5 cm^{-1}. The sample was piezo-scanned in three dimensions (PZT P-611.3S, Physik Instrumente, Karlsruhe, Germany). The acquisition time for a single multiplex CARS spectrum was 20 ms. A nonresonant reference signal was obtained by focusing either in glass (CH-stretch region) or in water (CC-stretch region). Unstained cells containing LDs were first imaged in bright field, and multiplex CARS images were taken of selected areas, typically covering 20 × 20 μm (50 × 50 pixels), where at each pixel a multiplex CARS spectrum was recorded, in both the CH-stretch region (−2800 to −3100 cm^{-1}) and CC-stretch region (−1400 to −1700 cm^{-1}) spectral range. All experiments (unless noted otherwise) were performed at room temperature.

Retrieval of spectral parameters

All measured multiplex CARS spectra were divided by the nonresonant reference signal, yielding a ''CARS signal strength'' that was independent of experimental parameters such as laser power or alignment (26). The phase

and amplitude of $\chi^{(3)}$ were determined using the MEM (24). For images, the signal/noise ratio (SNR) of spectra was increased by averaging every pixel phase and amplitude with all eight adjacent pixels. For the CC-stretch region, the error phase was determined using a third-order polynomial fit to the recovered phase, excluding the -1450 cm^{-1} and -1650 cm^{-1} resonances. After the error-phase subtraction, the imaginary part of the third-order nonlinear susceptibility (Im$\{\chi^{(3)}\}$) spectra was calculated. The spectra were fitted with three Lorentzians to determine C = C.

To derive spectral parameters unambiguously from the CH-stretch spectral region, the analysis was performed in several steps. In this way, possible ambiguities in determining the error phase for the whole spectrum were avoided. In a first approximation, the error phase was determined using a third-order polynomial fit to the retrieved phase, excluding the -2828 to -3000 cm^{-1} and -3005 to -3090 cm^{-1} frequency ranges. The amplitudes of the -2845 and -2880 cm^{-1} mode were determined using Voigt profile fits to the Im$\{\chi^{(3)}\}$ spectrum and local background subtraction. The CC$_{order}$ parameter followed directly from the calculated ratio I_{-2880}/I_{-2845}. Additional information on the retrieval of spectral parameters can be found in the Supplementary Material (Data S1, Movie S1).

Additional methods

All sample-preparation methods are described in the Supplementary Material (Data S1).

RESULTS

Quantitative determination of lipid unsaturation and physical state, using CARS

Coherent anti-Stokes Raman scattering is a nonlinear optical four-wave mixing process that is resonantly enhanced when the frequency difference between pump and Stokes matches a vibrational resonance of the sample (27). This resonant enhancement provides CARS with chemical and physical specificity, based on the inherent vibrational spectrum, without labeling. Here, we used CARS in the C-C and C-H stretching regions to quantify and characterize lipids noninvasively in LDs. In our multiplex CARS scheme, a broadband *Stokes* is used, in combination with a narrowband pump and probe, yielding an anti-Stokes spectrum (from a 0.3-μm^3 sample volume) that is generated simultaneously over a significant part (>300 cm^{-1}) of the vibrational spectrum. Using a phase-retrieval algorithm (see Methods), multiplex CARS spectra can be readily converted to Im$\{\chi^{(3)}\}$ spectra that are equivalent to the spontaneous Raman response (28), permitting quantitative analysis in terms of molecular concentrations.

Out of the wealth of molecularly specific information available in multiplex CARS microscopy, we focus on spectral parameters for two important LD characteristics: degree of fatty-acid unsaturation, and amount of acyl-chain order within droplets. The first parameter was obtained from a measurement of the local concentration of carbon double bonds. The second was derived from a vibrational resonance at $\sim$2880 cm^{-1}, characteristic of the amount of *trans-gauche* kinks along the acyl chains.

Fig. 1, a, c, and d, shows multiplex CARS measurements of different fatty-acid solutions in carbon tetrachloride (CCl$_4$). These results demonstrate the quantitative nature of multiplex
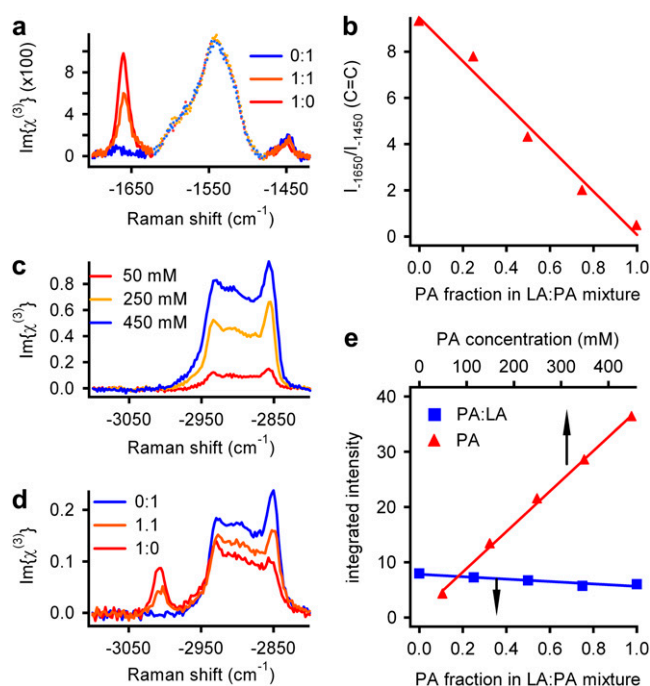

FIGURE 1 Illustration of quantitative nature of multiplex CARS. (*a*) Im$\{\chi^{(3)}\}$ spectra of LA/PA mixtures in CCl$_4$ in the CC-stretch spectral region. The PA/LA molar ratio is indicated. (*b*) C = C spectral parameter (I_{-1650}/I_{-1450}), as derived from spectra in *a*, as a function of C = C double-bond concentration. (*c* and *d*) Im$\{\chi^{(3)}\}$ spectra in CH-stretch vibrational region of different concentrations of PA in CCl$_4$, and of mixtures of PA and LA (100 mM total fatty-acid concentration) in CCl$_4$, respectively. (*e*) Integrated intensity of CH-stretch Im$\{\chi^{(3)}\}$ spectra of a concentration series of PA in CCl$_4$ (*red triangles*) and PA/LA mixtures in CCl$_4$ (*blue squares*; 100 mM total fatty-acid concentration).

CARS microscopy. Two vibrational frequency ranges are shown: from -1400 to -1700 cm^{-1} and from -2800 to -3100 cm^{-1}, denoted as ''CC-stretch'' and ''CH-stretch'', respectively. In Fig. 1 *a*, the total fatty-acid concentration is constant at 100 mM, and the concentration of C = C bonds was systematically varied, using different mixtures of palmitic acid (PA), which is fully saturated, and linolenic acid (LA), which has three C = C double bonds. The Im$\{\chi^{(3)}\}$ line shape was extracted directly from the measured multiplex CARS spectra, using a phase-retrieval algorithm based on the MEM (24,29). The resonances at ~-1650 cm^{-1} and -1450 cm^{-1} originated from the ν(C = C) stretching and δ(CH$_2$) deformation vibrations, respectively. The resonance centered at -1550 cm^{-1} is attributable to the CCl$_4$ solvent, and will be disregarded in the following text. The signal at -1650 cm^{-1} was directly proportional to the concentration of C = C bonds, and the -1450 cm^{-1} resonance can be used as a measure of total fatty-acid concentration (30). It is apparent from Fig. 1 *b* that the ratio I_{-1650}/I_{-1450} (denoted below as ''C = C'') provides a quantitative measure for the degree of lipid-chain unsaturation.

The interpretation of the CH-stretch vibrational region (Fig. 1, *c* and *d*) is complicated by the interaction, enhanced

by Fermi resonance, between CH-stretching fundamentals and overtones of $\delta(CH_2)$ deformation modes (31). The most dominant peaks, in this congested and complex spectral region, are those from the acyl-chain methylene symmetric (~-2845 cm^{-1}) and asymmetric (~-2880 cm^{-1}) stretch vibrations. The ratio I_{-2880}/I_{-2845} was shown to provide a measure for acyl-chain order (13) through its sensitivity to the amount of *gauche* kinks in the acyl chains and concomitant reduction in lateral chain-chain interactions (32). This ratio will be used to quantify the order of lipids (i.e., their fluidity) within LDs, and will be referred to as the parameter CC_{order}.

The integrated intensity of the complete CH-stretch vibrational spectrum provides a good measure of total fatty-acid concentration in pure PA dilutions (Fig. 1 *e*). Changing the fatty-acid composition (from PA to LA) is accompanied by significant spectral changes (Fig. 1 *d*). In particular, for LA, a vibrational resonance at ~-3020 cm,$^{-1}$ related to $=$C-H bond vibrations (33), appears, and the amplitude of the -2930 cm^{-1} spectral region increases relative to the -2845 cm^{-1} mode. In contrast to the C $=$ C stretch at -1650 cm^{-1}, the amplitude of the -3020 cm^{-1} ($=$ C-H stretch) resonance does not provide a reliable measure of acyl-chain unsaturation, presumably because of Fermi resonances (data not shown). It was verified that the integrated intensity in the C-H stretch region in fatty-acid mixtures provides a reliable indicator of total fatty-acid concentration (e.g., Fig. 1 *e*).

Spatial heterogeneity in unsaturation level and acyl-chain order in adipocyte LDs

Multiplex CARS imaging can be used to map quantitatively the spatial variations in the level of lipid unsaturation and acyl-chain order of different LDs within a single cell, or even within individual LDs. Fig. 2 *a* shows a bright-field image of an unstained 3T3-L1 adipocyte, incubated with a 1:3 mixture of LA and PA. The indicated area was imaged using multiplex CARS in both the CC-stretch and CH-stretch regions of the vibrational spectrum.

The local lipid concentration is represented by the integrated intensity of the Im$\{\chi^{(3)}\}$ spectrum in the C-H stretch region (Fig. 2 *d*). Typical Im$\{\chi^{(3)}\}$ spectra at the indicated positions are shown in Fig. 2, *b* and *c*, for the CC-stretch and CH-stretch regions, respectively. Although both the bright-field and multiplex CARS ''lipid concentration'' images show largely homogeneous LDs, the Im$\{\chi^{(3)}\}$ spectra at different spatial positions reveal significant variations in the local chemical composition of droplets. This spatial heterogeneity can be visualized using the C $=$ C parameter for contrast in the multiplex CARS image (Fig. 2 *e*). The local concentration of C $=$ C double bonds varies markedly between different LDs and, remarkably, even within a single LD. Fig. 2 *f* shows the multiplex CARS image of the same cell, displaying degrees of acyl-chain order. The CC_{order} and C $=$ C images show inverse contrast, affirming that in regions with fewer C $=$ C double bonds, the acyl chains are more ordered.

Fatty-acid composition is a major determinant of phase separation in adipocyte LDs

The rapid image-acquisition capability of multiplex CARS readily allows for analysis of individual LDs, within one cell, in different cells, or in cells grown under different incubation conditions. Such analysis provides information on both LD-to-LD and cell-to-cell variations, as well as statistically relevant averaged values for acyl-chain saturation level and order for specific incubation conditions. To illustrate this
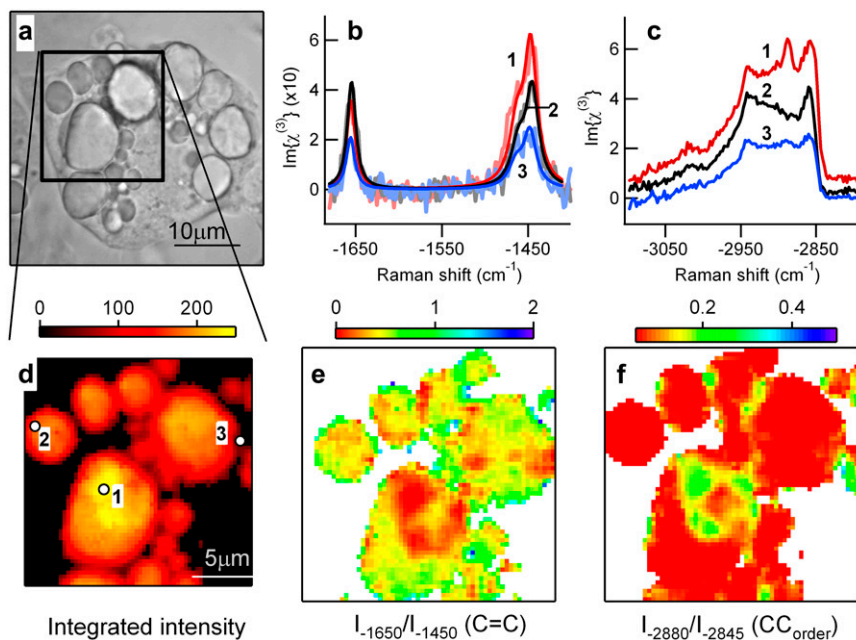

FIGURE 2 Multiplex CARS spectral imaging. (*a*) Bright-field image of an adipocyte incubated with a 1:3 mixture (mol/mol) of LA and PA. Marked region was imaged with multiplex CARS microscopy. Based on measured Im$\{\chi^{(3)}\}$ spectra at every pixel, images are derived with contrast based on (*d*) lipid concentration (integrated intensity), (*e*) C $=$ C concentration derived from CC-stretch region (I_{-1650}/I_{-1450}), and (*f*) acyl-chain order (I_{-2880}/I_{-2845}). (*b* and *c*) Representative Im$\{\chi^{(3)}\}$ spectra were recorded at locations indicated (in *d*) for CC-stretch and CH-stretch spectral regions, respectively. Least-squares fit of a sum of three Lorentzians to the data is also shown (*b*). Acquisition time was 20 ms for a multiplex CARS spectrum at every pixel position ($\sim$1 min/image).

unique capability, we performed and analyzed measurements of adipocytes, incubated with different mixtures of PA and LA. The results of these measurements are summarized in Fig. 3. Characteristic multiplex CARS images, representing local lipid concentration, local lipid order (CC$_{order}$), and local degree of unsaturation (C = C), are shown for each incubation mixture. Each data point in Fig. 3, *m* and *n*, corresponds to average values for the C = C and CC$_{order}$ parameters obtained from ~20 LDs originating from at least six different adipocyte cells.

It follows from Fig. 3, *m* and *n*, that for PA molar fractions ≤50% in the LA/PA incubation mixture, the C = C parameter is uniform over all LDs, and every local measurement accurately reflects the content of the incubation mixture: PA and LA are well-mixed within LDs, and homogeneously distributed over all LDs in all cells. Under these conditions, lipids are fluidized entirely within the LD. For higher PA fractions, however, phase separation occurs in some (but not all) LDs. In this regime, entirely homogeneous distributions, both in C = C and CC$_{order}$, are observed in the LDs of some cells, whereas other LDs, within the same cell or in other cells of the same sample, show a variation in C = C concentration and/or acyl-chain order. A variety of patterns therefore occurs. Remarkably, whereas incubation with pure PA mainly yielded entirely ordered LDs, fully fluidized LDs were also observed within the same cell (Fig. 3 *n*), although in all cases, the C = C parameter was consistent with an almost pure PA LD constitution (Fig. 3 *m*).

The mechanism of LD formation and growth

The mechanism of LD formation in adipocytes can be investigated by studies in which the fatty-acid composition of the incubation medium is changed from one fatty acid to another. Fig. 4 shows LDs in an adipocyte incubated with pure PA (for 96 h), followed by pure LA (for an additional 36 h). Whereas the large LD shows a low level of unsaturation (indicative of PA), most of the smaller LDs have significantly elevated levels of unsaturation. These results suggest that fatty acids such as LA, after cellular uptake, are preferentially used in the formation or growth of small LDs. At a later time, these small LDs probably fuse to the larger, mature LD (6).

Three-dimensional imaging of LDs

Multiplex CARS offers an inherent three-dimensional sectioning capability. The resolution in the lateral and axial directions is ~300 nm and ~1 μm, respectively (34). Such a
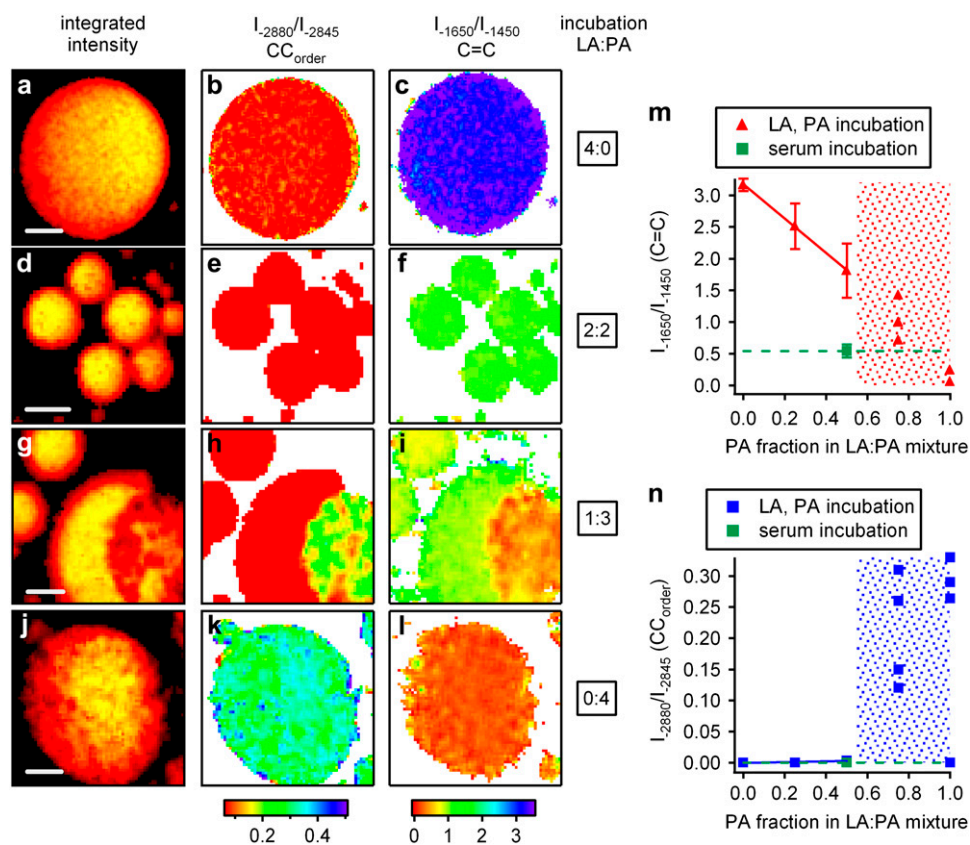

FIGURE 3 Lipid-droplet composition and packing dependent on incubation medium. Multiplex CARS images are shown for adipocytes incubated with different mixtures of LA and PA. Contrast in first column (*a*, *d*, *g*, and *j*) is based on lipid concentration (integrated intensity). In second (*b*, *e*, *h*, and *k*) and third (*c*, *f*, *i*, and *l*) columns, CC$_{order}$ (I_{-2880}/I_{-2845}) and C = C (I_{-1650}/I_{-1450}) parameters are displayed, respectively. (*m* and *n*) Values for C = C and CC$_{order}$ are given, respectively, averaged over ~20 LDs from at least six different adipocyte cells. For PA fractions ≤50%, LDs show homogeneous unsaturation and acyl-chain order levels. Error bars denote measured variation (1 SD). At PA fractions >50% (*m* and *n*, *shaded areas*), significant heterogeneity between and within LDs is evident, and only individual data points are shown. Because a variety of distribution patterns occurred for the latter incubation conditions, only *g*, *h*, *i*, *j*, k, and *l* are exemplary. Transition between homogeneous distributions of unsaturation and order parameters over LDs, and occurrence of heterogeneity within and/or between LDs, are indicated in *m* and *n* by shaded regions at elevated PA fractions. Dashed lines indicate reference value obtained for LDs formed in 3T3-L1 cells incubated in medium without added fatty acid (but containing 2% serum; see Methods). Scale bars, 5 μm.
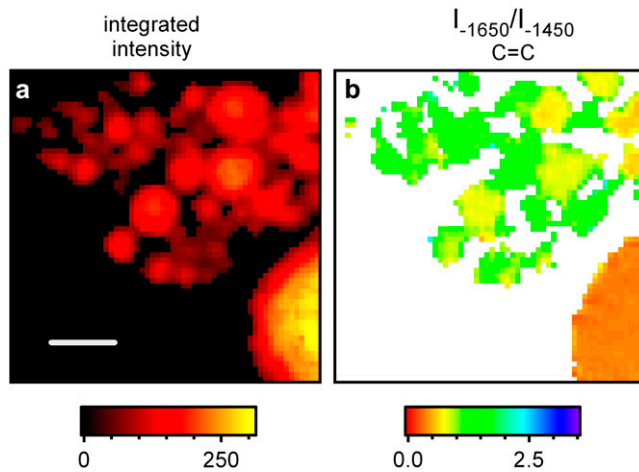
FIGURE 4 Fatty-acid uptake initially results in many small LDs. Multiplex CARS image of LDs in adipocyte after changing incubation medium from pure PA to pure LA. Contrast was based on (*a*) fatty-acid concentration, and (*b*) on $C = C$ (I_{-1650}/I_{-1450} intensity ratio). Scale bar, 5 μm.

three-dimensional data set (the Supplementary Material, Data S1, Movie S1) shows that even in cases of incubation with pure PA, individual LDs in adipocytes may display significant heterogeneity with respect to the CC_{order} parameter within the LD. Regions with significant acyl-chain order are next to regions that show highly disordered acyl chains. Three-dimensional imaging provides detailed information on the distribution of CC_{order} and $C = C$ within the LD, and permits volumetric measurements of the extent of phase separation.

DISCUSSION

Distinct vibrational markers were identified to quantify, within individual LDs, the spatial distribution of acyl-chain unsaturation (through the $C = C$ bond concentration) and the spatial distribution of acyl-chain order (in the CH-stretch region of the spectrum). We showed that these spectral markers, $C = C$ and CC_{order}, can be used to visualize the formation and growth of LDs, during the incubation of cells with different mixtures of saturated and unsaturated fatty acids. The fatty acids are taken up by the cells and efficiently esterified and stored as triacylglycerol in LDs. At low fractions of saturated fatty-acid PA, the LDs remain fluidized (i.e., large acyl-chain disorder). At high PA fractions (>50 mol % in a LA/PA mixture), however, phase separation is evident within LDs in some cases. Moreover, individual LDs may show increased acyl-chain order, whereas other LDs in the same cell are still completely fluidized. Generally, a decrease in acyl-chain order coincides with an increase in unsaturation level (higher $C = C$ bond concentration). It is apparent that the composition of the incubation medium is the single most important, but not sole, factor in determining lipid fluidity in the LD. Other effects that undoubtedly play a role involve the background of other fatty acids that are present in the cells before incubation, and potential metab-

olizing steps that may occur before or during triacylglycerol formation.

Lipid droplets have multiple and very diverse functions. Some of these functions are cell type specific, explaining the differences found between LDs of tissues such as adipose tissue, liver, and skeletal muscle. However, even within individual cells different LD subpopulations appear to exist. In adipocytes, perilipin, adipophilin, and TIP47-related proteins (PAT-family proteins) are not homogeneously distributed among the LDs, but are differentially present in LD subpopulations (35). Moreover, upon lipolytic activation, the hormone-sensitive lipase preferentially targets peripheral micro-LDs (36). Proteomics studies identified over 100 LD-associated proteins, including the LD-specific proteins of the PAT family, and also several membrane traffic-related proteins, underlining the likely importance of connections between intracellular membranes and LDs (37,38). Despite the apparent functional importance of LDs, much remains to be learned regarding LD dynamics, the local protein and lipid composition of LDs, and the interactions of LDs with other organelles, in particular in relation to the function of LDs in health and disease. The application of CARS demonstrated here enabled the label-free cellular imaging of lipid composition and packing of individual LDs. As such, it complements existing CARS approaches (17–23), and promises to be a very useful tool in LD research.

In the future, other areas of the vibrational spectrum may be addressed, possibly in combination with the use of deuterated incubation species (39), e.g., to assess quantitatively the distribution of cholesterylester, another abundant LD constituent. Furthermore, multiplex CARS microscopy can be combined with (multiphoton-absorption) fluorescence microscopy of live cells, to reveal the links between the local protein and lipid composition of LDs in relation to LD (mal)function.

SUPPLEMENTARY MATERIAL

To view all of the supplemental files associated with this article, visit www.biophysj.org.

REFERENCES

1. Murphy, D. J. 2001. The biogenesis and functions of lipid bodies in animals, plants and microorganisms. *Prog. Lipid Res.* 40:325–438.

2. Welte, M. A., S. Cermelli, J. Griner, A. Viera, Y. Guo, D. H. Kim, J. G. Gindhart, and S. P. Gross. 2005. Regulation of lipid-droplet transport by the perilipin homolog LSD2. *Curr. Biol.* 15:1266–1275.

3. Martin, S., and R. G. Parton. 2006. Lipid droplets: a unified view of a dynamic organelle. *Nat. Rev. Mol. Cell Biol.* 7:373–378.

4. Fernandez, M. A., C. Albor, M. Ingelmo-Torres, S. J. Nixon, C. Ferguson, T. Kurzchalia, F. Tebar, C. Enrich, R. G. Parton, and A. Pol.

2006. Caveolin-1 is essential for liver regeneration. *Science*. 313:1628–1632.

5. Welte, M. A. 2007. Proteins under new management: lipid droplets deliver. *Trends Cell Biol*. 17:363–369.

6. Boström, P., L. Andersson, M. Rutberg, J. Perman, U. Lidberg, B. R. Johansson, J. Fernandez-Rodriguez, J. Ericson, T. Nilsson, J. Borén, and S. O. Olofsson. 2007. SNARE proteins mediate fusion between cytosolic lipid droplets and are implicated in insulin sensitivity. *Nat. Cell Biol*. 9:1286–1293.

7. Petersen, K. F., and G. I. Shulman. 2006. Etiology of insulin resistance. *Am. J. Med*. 119:S10–S16.

8. Corcoran, M. P., S. Lamon-Fava, and R. A. Fielding. 2007. Skeletal muscle lipid deposition and insulin resistance: effect of dietary fatty acids and exercise. *Am. J. Clin. Nutr*. 85:662–667.

9. Bartz, R., W. H. Li, B. Venables, J. K. Zehmer, M. R. Roth, R. Welti, R. G. W. Anderson, P. S. Liu, and K. D. Chapman. 2007. Lipidomics reveals that adiposomes store ether lipids and mediate phospholipid traffic. *J. Lipid Res*. 48:837–847.

10. Tauchi-Sato, K., S. Ozeki, T. Houjou, R. Taguchi, and T. Fujimoto. 2002. The surface of lipid droplets is a phospholipid monolayer with a unique fatty acid composition. *J. Biol. Chem*. 277:44507–44512.

11. Chan, J. W., D. Motton, J. C. Rutledge, N. L. Keim, and T. Huser. 2005. Raman spectroscopic analysis of biochemical changes in individual triglyceride-rich lipoproteins in the pre- and postprandial state. *Anal. Chem*. 77:5870–5876.

12. Hellerer, T., C. Axang, C. Brackmann, P. Hillertz, M. Pilon, and A. Enejder. 2007. Monitoring of lipid storage in *Caenorhabditis elegans* using coherent anti-Stokes Raman scattering (CARS) microscopy. *Proc. Natl. Acad. Sci. USA*. 104:14658–14663.

13. Percot, A., and M. Lafleur. 2001. Direct observation of domains in model stratum corneum lipid mixtures by Raman microspectroscopy. *Biophys. J*. 81:2144–2153.

14. Rosch, P., H. Schneider, U. Zimmermann, W. Kiefer, and J. Popp. 2004. In situ Raman investigation of single lipid droplets in the water-conducting xylem of four woody plant species. *Biopolymers*. 74:151–156.

15. van Manen, H. J., Y. M. Kraan, D. Roos, and C. Otto. 2005. Single-cell Raman and fluorescence microscopy reveal the association of lipid bodies with phagosomes in leukocytes. *Proc. Natl. Acad. Sci. USA*. 102:10159–10164.

16. Whitley, A., and F. Adar. 2006. Confocal spectral imaging in tissue with contrast provided by Raman vibrational signatures. *Cytometry A*. 69A:880–887.

17. Xie, X. S., J. Yu, and X. Y. Yang. 2006. Living cells as test tubes. *Science*. 312:228–230.

18. Reference deleted in proof.

19. Huff, T. B., and J.-X. Cheng. 2007. In vivo coherent anti-Stokes Raman scattering imaging of sciatic nerve tissue. *J. Microsc*. 225:175–182.

20. Nan, X., J. X. Cheng, and X. S. Xie. 2003. Vibrational imaging of lipid droplets in live fibroblast cells with coherent anti-Stokes Raman scattering microscopy. *J. Lipid Res*. 44:2202–2208.

21. Nan, X., A. M. Tonary, A. Stolow, X. S. Xie, and J. P. Pezacki. 2006. Intracellular imaging of HCV RNA and cellular lipids by using simultaneous two-photon fluorescence and coherent anti-Stokes Raman scattering microscopies. *ChemBioChem*. 7:1895–1897.

22. Nan, X., E. O. Potma, and X. S. Xie. 2006. Nonperturbative chemical imaging of organelle transport in living cells with coherent anti-Stokes Raman scattering microscopy. *Biophys. J*. 91:728–735.

23. Heinrich, C., A. Hofer, A. Ritsch, C. Ciardi, S. Bernet, and M. Ritsch-Marte. 2008. Selective imaging of saturated and unsaturated lipids by wide-field CARS-microscopy. *Opt. Express*. 16:2699–2708.

24. Vartiainen, E. M., H. A. Rinia, M. Muller, and M. Bonn. 2006. Direct extraction of Raman line-shapes from congested CARS spectra. *Opt. Express*. 14:3622–3630.

25. DiDonato, D., and D. L. Brasaemle. 2003. Fixation methods for the study of lipid droplets by immunofluorescence microscopy. *J. Histochem. Cytochem*. 51:773–780.

26. Rinia, H. A., M. Bonn, and M. Müller. 2006. Quantitative multiplex CARS spectroscopy in congested spectral regions. *J. Phys. Chem. B*. 110:4472–4479.

27. Müller, M., and A. Zumbusch. 2007. Coherent anti-Stokes Raman scattering microscopy. *Chem. Phys. Chem*. 8:2156–2170.

28. Rinia, H. A., M. Bonn, M. Müller, and E. M. Vartiainen. 2007. Quantitative CARS spectroscopy using the maximum entropy method: the main lipid phase transition. *ChemPhysChem*. 8:279–287.

29. Vartiainen, E. M. 1992. Phase retrieval approach for coherent anti-Stokes Raman scattering spectrum analysis. *J. Opt. Soc. Am. B*. 9:1209–1215.

30. Davies, J. E. D., P. Hodge, F. D. Gunstone, and M. S. F. Lie Ken Jie. 1975. Raman studies of some diunsaturated olefinic and acetylenic fatty acids and their derivatives. *Chem. Phys. Lipids*. 15:48–52.

31. Schachtschneider, J. H., and R. G. Snyder. 1963. Vibrational analysis of the *n*-paraffins—II. Normal co-ordinate calculations. *Spectrochim. Acta [A]*. 19:117–168.

32. Devlin, M. T., and I. W. Levin. 1989. Raman spectroscopic studies of the packing properties of mixed dihexadecyl- and dipalmitoylphosphatidylcholine bilayer dispersions. *Biochemistry*. 28:8912–8920.

33. Verma, S. P., and D. F. H. Wallach. 1984. Raman spectroscopy of lipids and biomembranes. *In* Biomembrane Structure and Function. D. Chapman, editor. Verlag Chemie, Basel. 167–198.

34. Wurpel, G. W. H., J. M. Schins, and M. Müller. 2002. Chemical specificity in 3D imaging with multiplex CARS microscopy. *Opt. Lett*. 27:1093–1095.

35. Wolins, N. E., D. L. Brasaemle, and P. E. Bickel. 2006. A proposed model of fat packaging by exchangeable lipid droplet proteins. *FEBS Lett*. 580:5484–5491.

36. Moore, H. P. H., R. B. Silver, E. P. Mottillo, D. A. Bernlohr, and J. G. Granneman. 2005. Perilipin targets a novel pool of lipid droplets for lipolytic attack by hormone-sensitive lipase. *J. Biol. Chem*. 280:43109–43120.

37. Brasaemle, D. L., G. Dolios, L. Shapiro, and R. Wang. 2004. Proteomic analysis of proteins associated with lipid droplets of basal and lipolytically stimulated 3T3-L1 adipocytes. *J. Biol. Chem*. 279:46835–46842.

38. Liu, P., Y. Ying, Y. Zhao, D. I. Mundy, M. Zhu, and R. G. Anderson. 2004. Chinese hamster ovary K2 cell lipid droplets appear to be metabolic organelles involved in membrane traffic. *J. Biol. Chem*. 279:3787–3792.

39. Tong, L., Y. Lu, R. J. Lee, and J.-X. Cheng. 2007. Imaging receptor-mediated endocytosis with a polymeric nanoparticle-based coherent anti-Stokes Raman scattering probe. *J. Phys. Chem. B*. 111:9980–9985.